Improved synthetic–heterodyne Michelson interferometer vibrometer using phase and gain control feedback

Article *in* Applied Optics · December 2015

DOI: 10.1364/AO.54.010418

CITATIONS
8

READS
173

4 authors, including:

José Henrique Galeti
São Paulo State University
15 PUBLICATIONS **41** CITATIONS

SEE PROFILE

Michael Connelly
University of Limerick
131 PUBLICATIONS **1,549** CITATIONS

SEE PROFILE

applied optics

Improved synthetic-heterodyne Michelson interferometer vibrometer using phase and gain control feedback

José Henrique Galeti,[1] Cláudio Kitano,[1] and Michael J. Connelly[2,*]

[1]Universidade Estadual Paulista—UNESP, Department of Electrical Engineering, Avenida Brasil 56, 15385-000 Ilha Solteira, SP, Brazil
[2]Optical Communications Research Group, Department of Electronic and Computer Engineering, University of Limerick, Limerick, Ireland
*Corresponding author: michael.connelly@ul.ie

Received 24 September 2015; revised 9 November 2015; accepted 16 November 2015; posted 17 November 2015 (Doc. ID 250740); published 9 December 2015

Synthetic-heterodyne demodulation is a useful technique for dynamic displacement and velocity measurement using interferometric sensors as it can provide an output signal which is immune to interferometric drift. With the advent of cost effective, high-speed real-time signal processing systems and software, processing of the complex signals encountered in interferometry has become more feasible. In conventional synthetic-heterodyne demodulation schemes, to obtain the dynamic displacement or vibration of the object under test requires knowledge of the interferometer visibility and also the argument of two Bessel functions. In this paper, a new synthetic-heterodyne demodulation method is described leading to an expression for the dynamic displacement and velocity of the object under test that is significantly less sensitive to the received optical power. In addition, the application of two independent phase and gain feedback loops is used to compensate for the nonideal gain and phase response of the anti-aliasing filter required for the signal acquisition of the received wideband interferometer signal. The efficacy of the improved system is demonstrated by measuring the displacement sensitivity frequency response and linearity of a Piezoelectric Mirror-Shifter (PMS) over a range of 200 Hz–9 kHz. In addition, the system is used to measure the response of the PMS to triangular and impulse type stimuli. The experimental results show excellent agreement with measurements taken using two independent industry standard calibration methods.

OCIS codes: (120.0120) Instrumentation, measurement, and metrology; (120.3180) Interferometry; (120.3940) Metrology; (120.5050) Phase measurement; (120.7250) Velocimetry; (120.7280) Vibration analysis.

http://dx.doi.org/10.1364/AO.54.010418

1. INTRODUCTION

Optical interferometry can be used for sensitive measurement of displacement and velocity [1,2]. Recently a nonoptical technique, verified by laser Doppler vibrometry, has been used to measure the amplitude and phase of the dynamic displacement of a piezoelectric disk [3]. The basic principle of an interferometric displacement/velocity sensor is that an applied stimulus causes a phase shift between two light beams, which are combined and then converted to an electrical signal. This signal has a nonlinear relationship to the phase shift; thus, relatively complex signal processing techniques need to be applied to obtain an output signal that is linear proportional to the stimulus. Common techniques include pseudo-heterodyne [4], passive and active homodyne [5] and synthetic heterodyne [6]. The latter technique is particularly useful; since it also eliminates interferometric drift, whereby slow variations in the optical paths due to environmental influences cause the interferometry sensitivity to slowly vary. In all of this prior work, the demodulation process was implemented using analog circuits. In [7] we used a digital implementation (signal acquisition using an analog-to-digital converter) and signal processing to implement synthetic-heterodyne demodulation to measure the displacement of a 100 Hz vibrating reflective diaphragm in a low-finesse Fabry–Perot interferometer. Using the capabilities now available in cost-effective signal acquisition real-time signal processing systems, a self-correcting synthetic-heterodyne demodulation system was proposed and implemented, which overcomes the need for prior calibration [1]. Research on exploiting the advantages of digital signal processing to the synthetic-heterodyne demodulation is ongoing such as the work reported in [8].

In this paper a new synthetic-heterodyne demodulation scheme is proposed and implemented. The scheme uses two independent control loops applied to the laser diode

modulation current and the relative phase of two local oscillators required in the demodulation technique. The object under test is a Piezoelectric Mirror-Shifter (PMS). The scheme primary aims to directly obtain the displacement (in rad) and the velocity (in rad/s) without system parameter foreknowledge and secondarily to improve measurement accuracy. The frequency response of the PMS was measured up to 9 kHz. The linearity of the PMS was measured up to 200 nm displacement. The experimental results show significant improvement in accuracy in comparison to the previous scheme [1] and show improved agreement with data obtained using two alternative schemes: the signal coincidence method (SCM) [9] and the denominated n-Commuted Pernick method (n-CPM) [10]. From the measured frequency response a predicted response of a triangular input was compared with the measured output. The proposed control scheme uses two mutually independent control loops so that an arbitrary vibration can be demodulated. By using this capability the impulse response of the PMS was measured and its frequency content shows good agreement with that predicted using the calculated impulse response using a model of the PMS transfer function obtained using measurement of the PMS sinusoidal response.

2. THEORY AND IMPLEMENTATION

A schematic diagram of the sensor system under consideration is shown in Fig. 1. The optical source is a 658 nm wavelength stabilized single longitudinal mode visible laser diode (Ondax TO-658-PLR35) having a linewidth of 50 MHz and a side-mode suppression ratio >30 dB. The laser was operated at a bias current of 60 mA at which the output power is 20 mW. The laser current is amplitude modulated either by a single frequency $f_0 = 20$ kHz sine wave (using a modulation current amplitude I_{m0}) or with an additional $f_1 = 20$ Hz sine wave (using a modulation current amplitude I_{m1}). Both I_{m0} and I_{m1} are small (typically <5 mA) compared to the laser bias current so amplitude modulation induced variations in the laser power can be assumed to be negligible and are thereby neglected in the analysis. The collimated laser beam is input to a Michelson interferometer. The object under test is a Piezoelectric Mirror-Shifter (PMS) consisting of a mirror mounted on a piezoelectric actuator (Piezomechanik mirror-shifter STr-35), which is driven by a 1 MHz bandwidth high-voltage amplifier (Thorlabs HVA200). The PMS has a maximum displacement of 6 mm at the maximum permissible applied drive voltage of 150 V and an unloaded resonance frequency of 10 kHz. The beam width is 9 mm and the interference pattern period is 1.5 mm.

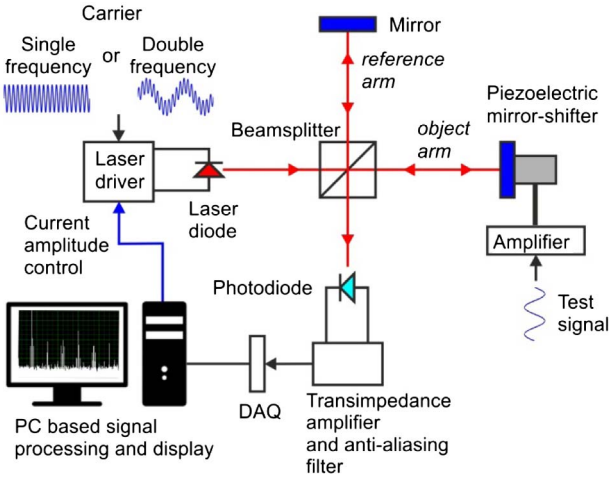

Fig. 1. Experimental setup.

The recombined reference and object light beams are detected by a photodiode (Thorlabs SM05PD2A—active area equal to 0.79 mm^2). and transimpedance amplifier (Stanford SR570 low-noise current amplifier), the output voltage of which is passed through a second order 100 kHz 3 dB bandwidth lowpass Anti-Aliasing Filter (AAF) before acquisition using a 16 bit resolution 250 kHz sampling rate Data Acquisition (DAQ) card (National Instruments USB-6211), which is also capable of signal generation. As described in section 3, the use of a low frequency modulation is used to compensate for the amplitude frequency response of the AAF. The acquired signal is processed in real-time using LabVIEW. The current modulation also causes modulation of the optical frequency. In the case of single frequency modulation and assuming an ideal AAF, the detected interferometric voltage signal at the DAQ input is given by,

$$v(t) = A + AV\cos[C_0\cos(2\pi f_0 t) + \phi(t) + \theta(t)], \quad (1)$$

where A is the average voltage, V the interferometer visibility, $\phi(t)$ is dynamic phase shift induced by the PMS dynamic displacement and $\theta(t)$ is a slowly varying phase shift caused by ambient fluctuations. C_0 is given by

$$C_0 = \frac{4\pi L}{c}\frac{d\nu}{di}I_{m0}, \quad (2)$$

where L is the nonzero mean path difference, c is the speed of light in free space, $d\nu/di$ is the sensitivity of the laser optical frequency with respect to current (~1.5 GHz/mA for the laser used in this work) [7]. A typical measured interferometric signal and its spectrum is shown in Fig. 2.

The dynamic phase shift $\phi(t)$ between the reference and test object beams, induced by the PMS dynamic displacement $x(t)$, is given by

$$\phi(t) = Kx(t). \quad (3)$$

The proportionality constant $K = 4\pi/\lambda$, where λ is the source wavelength. (1) can be expanded into a DC term plus an infinite series of carriers located at integer multiples of f_0, that are multiplied by either $\cos[\phi(t) + \theta(t)]$ or $\sin[\phi(t) + \theta(t)]$ [4,5],

$$\begin{aligned} v(t) = {} & A + AVJ_o(C_0)\cos[\phi(t)+\theta(t)] \\ & + 2AV\sum_{k=1}^{\infty}(-1)^k J_{2k}(C_0)\cos(4\pi k f_0 t)\cos[\phi(t)+\theta(t)] \\ & - 2AV\sum_{k=0}^{\infty}(-1)^k J_{2k+1}(C_0)\cos[2\pi(2k+1)f_0 t] \\ & \times\sin[\phi(t)+\theta(t)]. \end{aligned} \quad (4)$$

$J_j(C_0)$ are Bessel functions of the first kind of order j with argument C_0. In synthetic-heterodyne demodulation any two terms in Eq. (4) with $\cos[\phi(t) + \theta(t)]$ and $\sin[\phi(t) + \theta(t)]$ can be processed to obtain a signal proportional to the time rate of

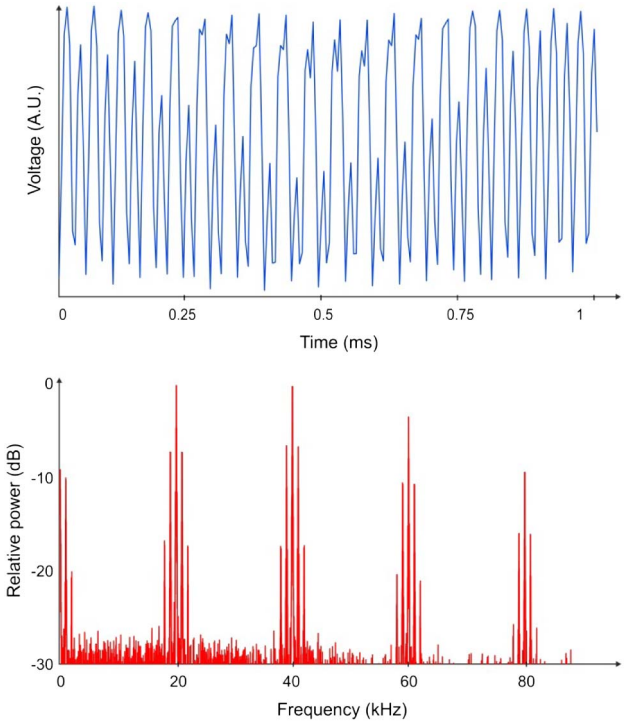

Fig. 2. Top: typical measured interferometric signal after acquisition. Bottom: its spectrum. The vibration frequency is 1 kHz.

change of $\phi(t)$. As previously described, by a process of multiplying Eq. (4) by local oscillators $\cos(2\pi f_0 t)$, $\cos(4\pi f_0 t)$ and subsequent lowpass filtering, the following signals are obtained [1,6],

$$S_1(t) = -AVJ_1(C_0)\sin[\phi(t) + \theta(t)] \tag{5}$$

and

$$S_2(t) = -AVJ_2(C_0)\cos[\phi(t) + \theta(t)]. \tag{6}$$

Defining $S_3(t) = S_2 dS_1/dt - S_1 dS_2/dt$ gives

$$S_3(t) = (AV)^2 J_1(C_0)J_2(C_0)\dot{\phi}(t), \tag{7}$$

where it is assumed that $d\theta/dt \ll d\phi/dt$. In the case of small displacement, the maximum deviation of the interferometric signal Eq. (1) from its average value is guaranteed for $C_0 \geq \pi$, in which case AV is obtained as a long-term average, typically over a time span equal to 2000 periods of f_0, of half the difference between the maximum and minimum of $v(t)$. In our previous work C_0 was measured and I_{m0} was adjusted to set $C_0 = 4.44$ at which $|J_1(C_0)J_2(C_0)|$ is at its maximum value of 0.051, for $C_0 > \pi$ [1]. By dividing Eq. (7) by the measured $(AV)^2 J_1(C_0)J_2(C_0)$, a signal equal to $\dot{\phi}(t)$ is obtained. In the experimental setup of [1], the time variation of AV was slow. In a less mechanically stable setup or where the object under test reflectivity varies with time, the received optical power and visibility can vary significantly with time, leading to undesired fluctuations in the measured $\dot{\phi}(t)$ caused by error in the division of the instantaneous value of $(AV)^2$ factor in Eq. (7) by its long-term average. It is therefore desirable to obtain a signal proportional to $\dot{\phi}(t)$, which is effectively independent of AV. Defining $S_v(t) = S_3/(S_1^2 + S_2^2)$ gives

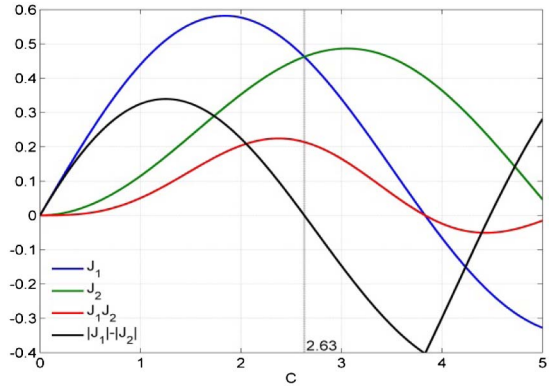

Fig. 3. Bessel functions and combinations.

$$S_v(t) = \frac{J_1(C_0)J_2(C_0)\dot{\phi}(t)}{J_1^2(C_0)\sin^2\phi(t) + J_2^2(C_0)\cos^2\phi(t)}. \tag{8}$$

When $C_0 = 2.63$, $J_1(C_0) = J_2(C_0)$ and $J_1(C_0)J_2(C_0) = 0.21$ which is very close to its maximum possible value of 0.22 as shown in Fig. 3. Setting C_0 to this desired value can be achieved using a feedback loop as described in section 3. When $C_0 = 2.63$, the demodulated output signal obtained from (8), becomes

$$S_v(t) = \dot{\phi}(t), \tag{9}$$

which is directly proportional to the velocity $\dot{x}(t)$, self-calibrated and independent of ambient fluctuations and AV, which improves measurement stability and accuracy. The object relative displacement $x(t)$ to that at some reference time t_0 can be obtained as

$$x(t) = \frac{1}{K}\int_{t_0}^{t} S_v(t)\mathrm{d}t. \tag{10}$$

The lower operational value of C_0 requires a lower modulating current for the same cavity length, which reduces the effect of laser power modulation. Also the SNR is improved because of the increased value of $|J_1(C_0)J_2(C_0)|$ from 0.051 to 0.21.

The above analyses assume that the optical receiver and AAF have frequency independent gain and phase responses, which is not strictly true in practice. In this work the optical receiver bandwidth is very high and the AAF frequency response is dominant. Even though it is possible to design an AAF which has a flat amplitude response in the passband, the associated phase response is a function of frequency, which can impact on the accuracy of both of the above techniques. The phase and gain response of the AAF can be compensated for by using two independent feedback loops as described in the next section.

3. PHASE AND GAIN FEEDBACK CONTROL

A schematic of the signal processing algorithm and control loops is shown in Fig. 4.

If the AAF frequency response is considered, the correct form of Eq. (1), assuming the bandwidth of $\cos[\phi(t)]$ and $\sin[\phi(t)]$ is $\ll f_0$, can be expressed as Eq. (4), with the inclusion of the frequency dependent gain and phase, and including the additional low frequency current modulation frequency f_1,

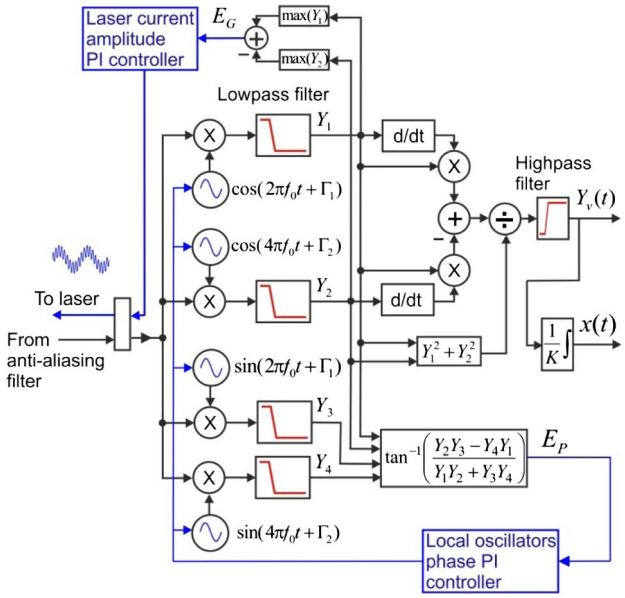

Fig. 4. Signal processing and control loops schematic diagram.

$$v(t) = A + AVJ_o(C_0)\cos[C_1\cos(2\pi f_1 t) + \phi(t) + \theta] + 2AV\sum_{k=1}^{\infty}(-1)^k G_{2k}J_{2k}(C_0)\cos[4k\pi f_0 t + \psi_{2k}] \times \cos[C_1\cos(2\pi f_1 t) + \phi(t) + \theta] - 2AV\sum_{k=0}^{\infty}(-1)^k G_{2k+1}J_{2k+1}(C_0) \times \cos[2\pi(2k+1)f_0 t + \psi_{2k+1}] \times \sin[C_1\cos(2\pi f_1 t) + \phi(t) + \theta(t)], \quad (11)$$

where G_j and ψ_j are the receiver voltage gain, relative to that at DC, and the induced phase shift, respectively, at frequency jf_0 and $C_1 = (4\pi L/c)I_{m1}d\nu/di$. The additional low frequency modulation current amplitude is set such that C_1 is $\geq\pi$ so the peak-to-peak value of $v(t)$ is always equal to its maximum possible value of $2AV$. This provides a mechanism to produce a feedback signal that is used to compensate for the AAF amplitude response.

As before the terms in Eq. (11) centered at frequencies f_0 and $2f_0$ are multiplied with local oscillators $\cos(2\pi f_0 t + \Gamma_1)$ and $\cos(4\pi f_0 t + \Gamma_2)$, respectively, where Γ_1 and Γ_2 are controllable phases, and then low-pass filtered to give signals Y_1 and Y_2

$$Y_1(t) = -AVG_1J_1(C_0)\sin[\phi(t) + \Psi(t)]\cos(\psi_1 - \Gamma_1) \quad (12)$$

and

$$Y_2(t) = -AVG_2J_2(C_0)\cos[\phi(t) + \Psi(t)]\cos(\psi_2 - \Gamma_2), \quad (13)$$

where $\Psi(t) = C_1\cos(2\pi f_1 t) + \theta(t)$. Similarly if the terms in Eq. (11) centered at frequencies f_0 and $2f_0$ are multiplied with local oscillators $\sin(2\pi f_0 t + \Gamma_1)$ and $\sin(4\pi f_0 t + \Gamma_2)$, respectively, and low-pass filtered, to get signals Y_3 and Y_4,

$$Y_3(t) = AVG_1J_1(C_0)\sin[\phi(t) + \Psi(t)]\sin(\psi_1 - \Gamma_1) \quad (14)$$

and

$$Y_4(t) = AVG_2J_2(C_0)\cos[\phi(t) + \Psi(t)]\sin(\psi_2 - \Gamma_2). \quad (15)$$

A phase error signal can be defined as $E_P = (\psi_1 - \Gamma_1) - (\psi_2 - \Gamma_2)$, which can be obtained as

$$E_P = \tan^{-1}\left(\frac{Y_2(t)Y_3(t) - Y_4(t)Y_1(t)}{Y_1(t)Y_2(t) + Y_3(t)Y_4(t)}\right), \quad (16)$$

which is independent of A, V, $G_{1,2}$, $J_{1,2}(C_0)$ and $\Psi(t) + \phi(t)$. The phase ratio $K = \psi_2/\psi_1$, is never equal to 1 for all AAF filters. In particular for frequencies less than the 3 dB cut-off frequency, K can be assumed to be equal to 2. Setting $\Gamma_1 = K\Gamma_2$, E_P can be written as

$$E_P = (K - 1)(\Gamma_1 - \psi_1). \quad (17)$$

A proportional–integration (PI) control loop was used to control Γ_1 such that $E_P = 0$, so Y_1 and Y_2 become

$$Y_5(t) = -AVG_1J_1(C_0)\sin[\Psi(t) + \phi(t)] \quad (18)$$

and

$$Y_6(t) = -AVG_2J_2(C_0)\cos[\Psi(t) + \phi(t)]. \quad (19)$$

Calculating $Y_7(t) = Y_5\dot{Y}_6 - Y_6\dot{Y}_5$ gives

$$Y_7(t) = (AV)^2G_1G_2J_1(C_0)J_2(C_0)(\dot{\Psi} + \dot{\phi}). \quad (20)$$

However, it is desirable to obtain a signal proportional to $\dot{\phi}(t)$ that is less sensitive to or independent of AV. $Y_v(t) = Y_7/(Y_5^2 + Y_6^2)$ is given by

$$Y_v(t) = \frac{G_1G_2J_1(C_0)J_2(C_0)[\dot{\Psi}(t) + \dot{\phi}(t)]}{G_1^2J_1^2(C_0)\sin^2[\Psi(t) + \phi(t)] + G_2^2J_2^2(C_0)\cos^2[\Psi(t) + \phi(t)]}. \quad (21)$$

By setting C_0 to an appropriate value, Eq. (21) will be equal to $\dot{\Psi}(t) + \dot{\phi}(t)$. This can be achieved by suitable control of I_{m0} using a feedback loop. Defining a gain error signal

$$E_G = AV[G_1J_1(C_0) - G_2J_2(C_0)]. \quad (22)$$

$Y_5(t)$ and $Y_6(t)$ will attain peak values of $AVG_1J_1(C_0)$ and $AVG_2J_2(C_0)$, respectively, when $C_1 \geq \pi$, which can be achieved using a suitable modulation current I_{m1}. $AVG_1J_1(C_0)$ and $AVG_2J_2(C_0)$ can be measured from the peak values of $Y_5(t)$ and $Y_6(t)$ over a time span equal to or exceeding the period of f_1. A PI control loop was used to control I_{m0} (and thereby C_0) such that $E_G = 0$, in which case Eq. (21) becomes

$$Y_v(t) = \dot{\Psi}(t) + \dot{\phi}(t). \quad (23)$$

By applying a highpass filter to Eq. (23), the ambient and low frequency modulation can be eliminated, giving

$$Y_v(t) = \dot{\phi}(t). \quad (24)$$

Hence, $x(t)$ and $\dot{x}(t)$ can be calculated with the limitation that it is not possible to detect displacement frequencies $<f_1$. Equation (24) is identical to Eq. (9), which was obtained for an ideal system. The velocity is then calculated as

$$\dot{x}(t) = \frac{Y_v(t)}{K} \quad (25)$$

and the displacement as

$$x(t) = \frac{1}{K}\int Y_v(t)\mathrm{d}t. \tag{26}$$

4. EXPERIMENTAL RESULTS

The implemented control loop requires a low frequency (20 Hz) current modulation $I_{m1} = 0.6$ mA applied to the laser current driver to obtain $C_1 \geq \pi$ in a 2 cm mean path difference cavity. Typical $Y_5(t)$ and $Y_6(t)$ signals that occur when $E_G = 0$ are shown in Fig. 5. When both error signals are equal to zero, $Y_5(t)$ and $Y_6(t)$ have identical amplitudes but with a 90 degree relative phase shift. The quadrature nature of these signals when this situation occurs is shown in Fig. 6.

The system was used to measure the PMS sensitivity (displacement amplitude divided by the applied voltage in nm/Volt) small-signal frequency response and linearity. A typical demodulated 9 kHz vibration velocity signal $Y_v(t)$ is shown in Fig. 7. The demodulated signals at lower frequencies are of similar quality.

The measured PMS response at three frequencies is shown in Fig. 8. Showing good linearity over a 0 to 50 V range of drive voltage amplitudes.

By way of comparison, the measured frequency response of the proposed scheme (Syn-c) was compared with

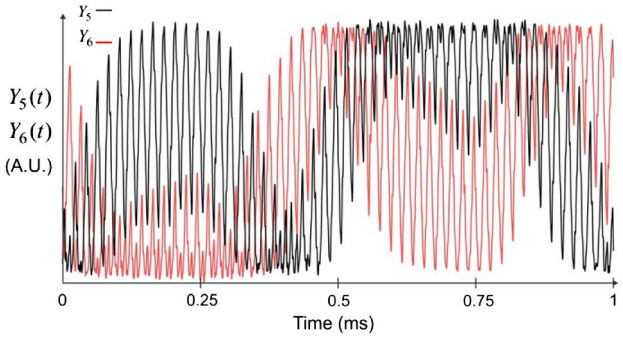

Fig. 5. Typical $Y_5(t)$ and $Y_6(t)$ signals.

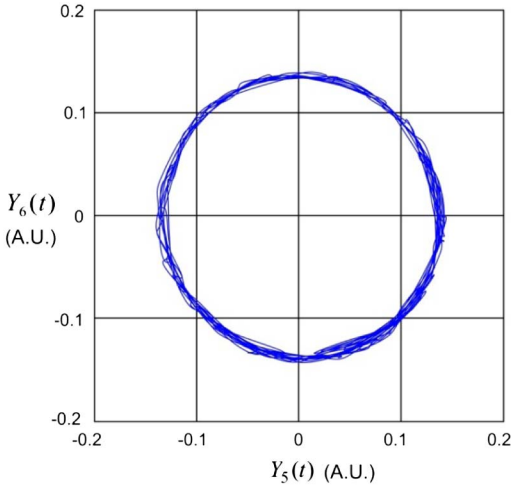

Fig. 6. $Y_6(t)$ versus $Y_5(t)$ showing their quadrature nature when the gain and phase control error signals are zero.

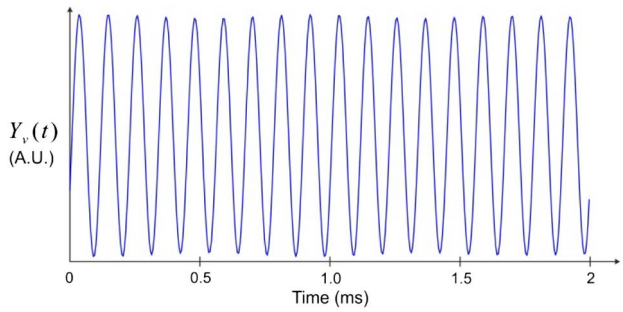

Fig. 7. Demodulated 9 kHz vibration signal.

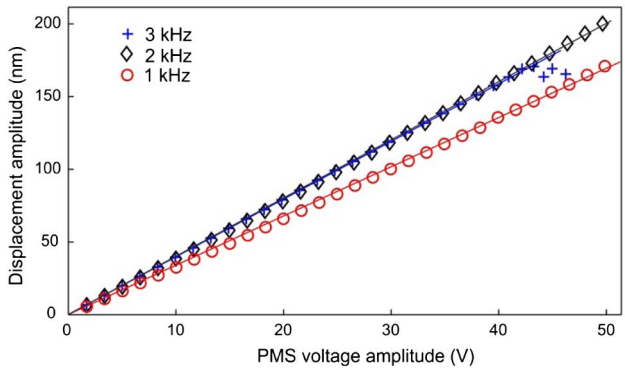

Fig. 8. PMS frequency response.

measurements obtained using two independent measurement procedures: (a) the SCM, whose application is detailed in ISO 16063-41 [11], is an applicable modification of the standard for primary vibration calibration ISO 16063-11 [12], which is described in detail in [9] and (b) the denominated n-CPM [10]. This latter method uses the magnitude spectrum of the photodetected signal from the interferometer with no carrier modulation applied. In the case of sinusoidal vibration, the photodetected signal (neglecting slow and small ambient fluctuations in phase) is given by

$$w(t) = A + AV\ \cos[\phi_0\ \cos(2\pi f t)]. \tag{27}$$

If V_1, V_2, V_3… are the harmonic magnitudes of the fundamental and the higher order harmonics of $w(t)$, and the harmonic with maximum magnitude V_n, then ϕ_0 can be determined from

$$\phi_0^2 = \frac{4(n+1)(n+2)(n+3)|V_{n+2}|}{(n+3)|V_n| + 4(n+2)|V_{n+2}| + (n+1)|V_{n+4}|}, \tag{28}$$

and then x_0 can be obtained directly from Eq. (3). The measured small-signal sensitivity is shown in Fig. 9. For the voltage amplitudes used there was negligible harmonic distortion indicating operation in the linear regime. The experimental results using SCM and n-CPM agree well with the synthetic-heterodyne data. The PMS exhibits a strong resonance at a frequency of approximately 6.3 kHz.

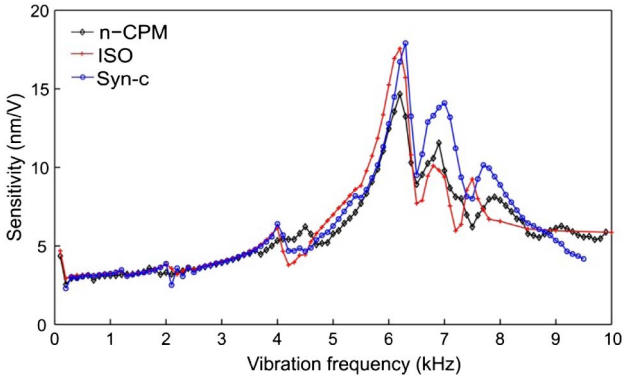

Fig. 9. PMS sensitivity frequency response.

The measured response obtained in our previous work [1] (Syn-het) was compared with measurements obtained using the proposed control scheme (Syn-c) and are shown in Fig. 10; the improvement can be clearly seen.

Although the previous methods (SCM and n-CPM) are appropriate to accurately measure the frequency response of the PMS they are not time domain based methods, i.e., is not possible to apply an arbitrary waveform to the input and obtain the corresponding time domain response. The proposed method is able to measure the frequency response characteristic in a single measurement by applying a pulse signal and measuring the PMS response as shown in Fig. 11 for a 200 Hz pulse stream with a pulse width of 50 μs. The frequency response can be

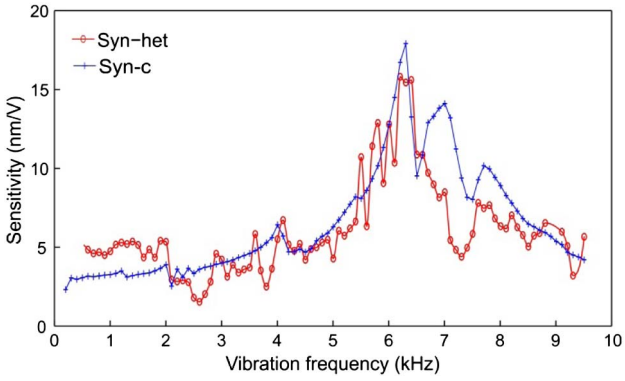

Fig. 10. PMS sensitivity frequency comparison.

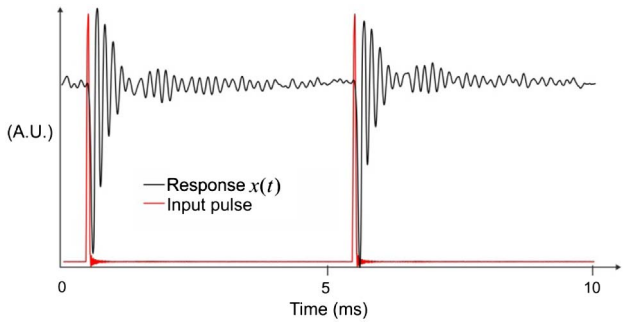

Fig. 11. PMS impulse response.

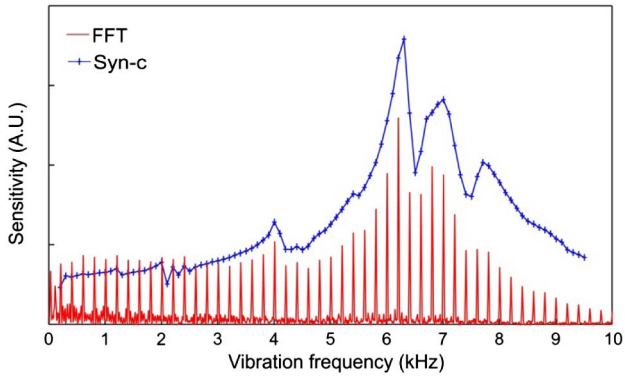

Fig. 12. PMS sensitivity frequency response and pulse response FFT.

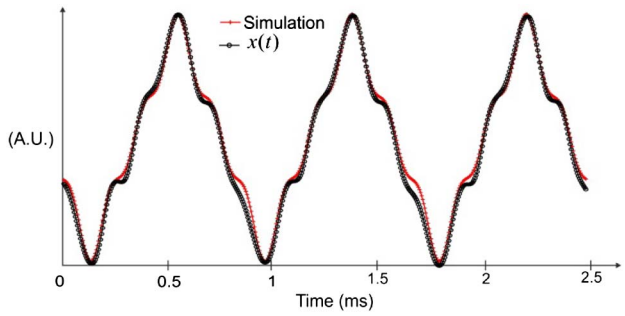

Fig. 13. Demodulated 1.2 kHz triangular displacement signal and simulation.

determined by computing the Fast Fourier Transform (FFT) of the measured response as shown in Fig. 12. The envelope of the frequency response obtained using the FFT of the impulse response is very similar to that obtained using a frequency sweep.

The measured sensitivity magnitude and phase was used to model the PMS displacement transfer function. A simulated triangular response was obtained by using the modeled transfer function and compared to the measured response $x(t)$ by applying a 1.2 kHz triangular wave to the PMS input as shown in Fig. 13.

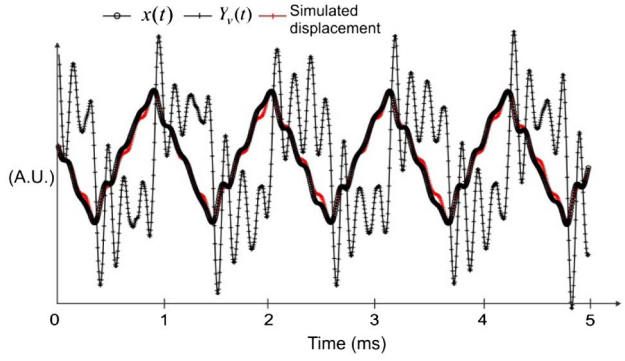

Fig. 14. Demodulated signals $x(t)$, $Y_v(t)$ and the simulated displacement for a 900 kHz applied triangular stimulus.

A 900 Hz triangle wave was applied to the PMS. The measured velocity $Y_v(t)$ is highly affected by the 7th harmonic (6.3 kHz), which is close to the PMS resonant frequency. As shown in Fig. 14, the measured velocity is quite different from the constant velocity expected from a nonresonant PMS.

5. CONCLUSIONS

A new digital synthetic-heterodyne demodulation scheme was implemented in real-time using fast signal acquisition and processing. The use of two independent control loops results in significant improvements in the stability and accuracy of the detected dynamic displacement and velocity. The system was successfully used to measure the frequency response of a mirror-shifter and the results show good agreement with measurements taken using the n-CPM and SCM techniques.

Funding. CAPES Foundation, Ministry of Education of Brazil (7730-14-4); CNPq National Council of Research and Development, Brazil (478817/2012-6); Enterprise Ireland (CFTD/07/IT/312b).

Acknowledgment. This research was carried out while José Henrique Galeti was a visiting researcher in the Optical Communications Research Group at the University of Limerick.

REFERENCES

1. M. J. Connelly, J. H. Galeti, and C. Kitano, "Michelson interferometer vibrometer using self-correcting synthetic-heterodyne demodulation," Appl. Opt. **54**, 5734–5738 (2015).
2. J. H. Galeti, R. T. Higuti, E. C. N. Silva, and C. Kitano, "Nanodisplacement measurements of piezoelectric flextensional actuators using a new interferometry homodyne method," IEEE Trans. Instrum. Meas. **64**, 1256–1265 (2015).
3. N. Pérez, R. C. Carbonari, M. A. B. Andrade, F. Buiochi, and J. C. Adamowski, "A FEM-based method to determine the complex material properties of piezoelectric disks," Ultrasonics **54**, 1631–1641 (2014).
4. D. A. Jackson, A. D. Kersey, M. Corke, and J. D. Jones, "Pseudo-heterodyne detection scheme for optical interferometers," Electron. Lett. **18**, 1081–1083 (1982).
5. A. Dandridge, A. B. Tveten, and T. G. Giallorenzi, "Homodyne demodulation scheme for fiber optic sensors using phase generated carrier," IEEE J. Quantum Electron. **18**, 1647–1653 (1982).
6. J. H. Cole, B. A. Danver, and J. A. Bucaro, "Synthetic-heterodyne interferometric demodulation," IEEE J. Quantum Electron. **18**, 694–697 (1982).
7. M. J. Connelly, "Digital synthetic-heterodyne interferometric demodulation," J. Opt. A **4**, S400–S405 (2002).
8. A. V. Kudryashov, L. B. Liokumovich, and A. V. Medvedev, "Digital demodulation methods for fiber interferometers," Opt. Mem. Neural Netw. **22**, 236–243 (2013).
9. H. J. von Martens, "Expanded and improved traceability of vibration measurements by laser interferometry," Rev. Sci. Instrum. **84**, 121601 (2013).
10. J. H. Galeti, P. L. Berton, C. Kitano, R. T. Higuti, R. C. Carbonari, and E. C. N. Silva, "Wide dynamic range homodyne interferometry method and its application for piezoactuator displacement measurements," Appl. Opt. **52**, 6919–6930 (2013).
11. "Methods for the calibration of vibration and shock transducers—Part 41: calibration of laser vibrometers" ISO 16063-41:2011 (International Organization for Standardization (ISO), 2011).
12. "Methods for the calibration of vibration and shock transducers—Part 11: primary vibration calibration by laser interferometry" ISO 16063-11:1999 (International Organization for Standardization (ISO), 1999).